JOURNAL OF CATALYSIS 78, 341–351 (1982)

Mg- and Si-Doped Iron Oxides for the Photocatalyzed Production of Hydrogen from Water by Visible Light (2.2 eV $\leq h\nu \leq$ 2.7 eV)

C. LEYGRAF, M. HENDEWERK, AND G. A. SOMORJAI

Materials and Molecular Research Division, Lawrence Berkeley Laboratory, and Department of Chemistry, University of California, Berkeley, California 94720

Received July 9, 1982; revised August 18, 1982

Connected polycrystalline discs of Mg-doped (p-type) and Si-doped (n-type) iron oxides produced hydrogen from water using light in the solar range (2.2 eV $\leq h\nu \leq$ 2.7 eV) and in the absence of any external potential. In 0.1 *M* Na_2SO_4 or in 0.01 *N* NaOH solutions the device produces hydrogen catalytically with rates of 1–2 H_2 monolayers per minute.

1. INTRODUCTION

The photoinduced dissociation of water to produce hydrogen and oxygen has been the subject of intense research in recent years. One direction of these investigations is to explore the use of semiconducting anodes (e.g., n-type $SrTiO_3$ or TiO_2) and cathodes (e.g., p-type GaP) to generate oxygen and hydrogen, respectively in aqueous solutions. A drawback of many systems studied is the need to employ uv radiation (e.g., with $SrTiO_3$ or TiO_2) since the band gaps of these compounds are around 3 eV or higher and band gap or larger photon energies are needed to generate the electron hole pairs that are utilized for the reduction of H^+ and for the oxidation of OH^-. Another difficulty in some cases (e.g., in GaP, MoS_2, or PtS_2) is the requirement of single crystals for efficient power conversion efficiencies.

In order to employ solar energy for the photodissociation of water, materials with band gaps in the solar range are needed. Iron oxides certainly fulfill this requirement. The band gap of α-Fe_2O_3 is 2.2 eV and thus much of the solar radiation can be utilized.

Photoelectrochemical studies aimed at the dissociation of water using iron oxide as the anode have indicated that an external potential of about 0.6 to 0.7 eV is needed in addition to irradiation by light of greater than band gap energy (*1*). Earlier studies have shown that one way to reduce or possibly eliminate the need of an external potential is to use photochemical diode cells consisting of both p- and n-type semiconductors as photoactive materials (*2*). A few p/n diode cells have been reported in which photodissociation of water was actually achieved without the need of an external bias (*2–5*). Whereas a large number of n-type Fe_2O_3 photoelectrodes have been successfully used, no p-type Fe_2O_3 has so far shown satisfactory photocatalytic behavior (*6*).

We report here the photodissociation of water by a polycrystalline p/n diode assembly which is solely based on iron oxide electrodes and in the absence of external potential. The p- and n-type iron oxides have been synthesized using MgO and SiO_2, respectively, as dopants. The photoinduced splitting is observed using light in the solar range of the electromagnetic spectrum and at ambient temperature and in aqueous solutions with pH ranging from 6 to 14. Photogenerated hydrogen has been detected by gas chromatography in rates of about 1–2 monolayers/min (10^{15} H_2 molecules/min) that were sustained for 3 days. It appears that the inexpensive, polycrystalline doped iron oxides may serve as economical catalysts for the conversion of solar energy to storable hydrogen.

0021-9517/82/120341-11$02.00/0

2. EXPERIMENTAL

The samples were prepared by mixing powders of α-Fe_2O_3, SiO_2, and MgO, all with a nominal purity of 99.9% or better. The mixed powders were pressed (7000 kg/cm^2) to form pellets 10 mm in diameter which were then sintered in air at 1340–1390°C for at least 20 hr. By sintering the pellets in this temperature region and by subsequent rapid cooling the resistivity of the mixed oxides was lowered. The resulting Si-doped pellets had dark resistivities of $\sim 10^3$ to $10^4\ \Omega \cdot$ cm.

Sample characterization by means of X-ray analysis, SEM, and scanning AES showed the Si-doped samples to be heterogeneous with two phases: an Si-doped Fe_2O_3 matrix and a highly enriched Si phase. The Mg-doped samples consist mainly of a Mg-doped Fe_2O_3 matrix. A scanning electron microscopy picture of the pellets surface morphology is shown in Fig. 1. A summary of the results of sample characterization is given in Table I.

The photoelectrochemical and photochemical experiments were conducted in the apparatus illustrated in Fig. 2. It consists of an electrochemical cell for measurements of current–potential curves and a closed circulation loop passing above the solution for transporting H_2 gas produced from the cell to a gas chromatograph where the amount of hydrogen produced is detected. For standard photoelectrochemical studies the cell is filled with a water solution in which the sample, a Pt counter electrode, and a Mercuric Oxide Luggin capillary reference electrode are immersed. The cell is further fitted with a quartz window for illuminating the sample and with provisions for inert gas inlet and outlet. All voltage readings are presented vs the reversible hydrogen electrode (RHE). Current–voltage curves obtained in the dark and under illumination were obtained using a

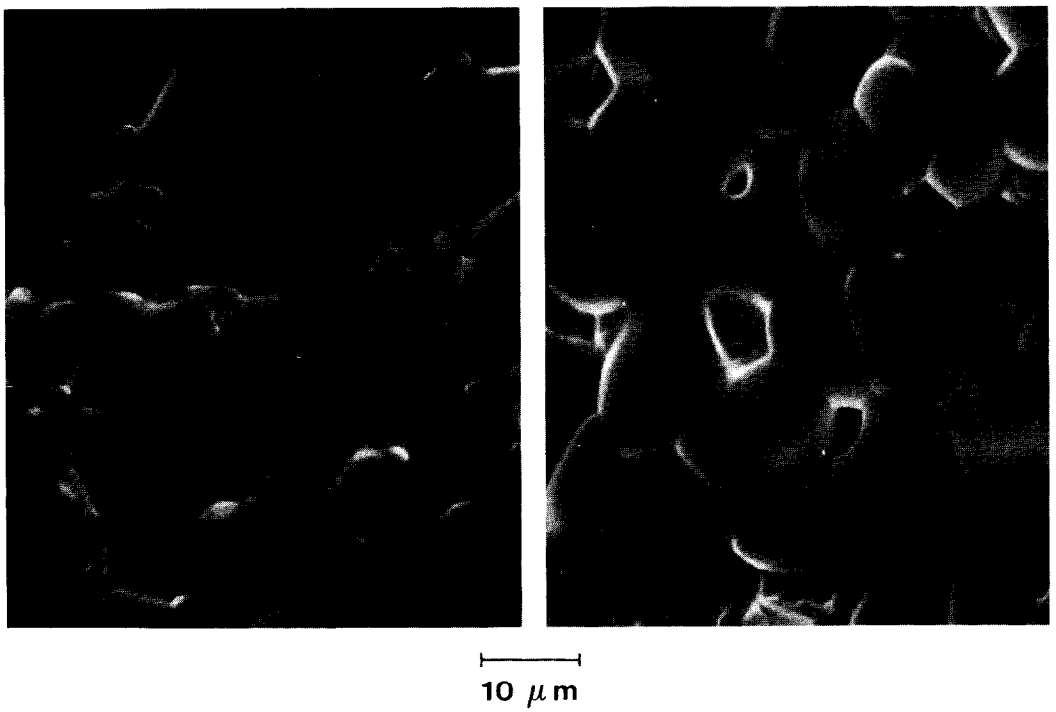

FIG. 1. Scanning electron microscopy photographs of n-type Si-doped iron oxide (left) and p-type Mg-doped iron oxide (right). The dopant levels are Si/(Si + Fe) = 2 atom% and Mg/(Mg + Fe) = 1 atom%.

TABLE 1

Sample Characterization of Doped Iron Oxides

Sample	Type	Fe_2O_3 Matrix		Precipitates Si	Resistivity ($\Omega \cdot$ cm)
		Si / Si + Mg + Fe [atom%]	Mg / Si + Mg + Fe [atom%]	Si / Si + Fe + Mg [atom%]	
Si/(Si + Fe) = 1 atom%	n	≤1	—	80–90	10^3
Si/(Si + Fe) = 2 atom%	n	1	—	80–90	10^3
Si/(Si + Fe) = 10 atom%	n	5–6	—	90–100	10^3–10^4
Si/(Si + Fe) = 20 atom%	n	7–8	—	90–100	10^4
Mg/(Mg + Fe) = 1 atom%	p	—	≤1	—	10^4–10^5
Mg/(Mg + Fe) = 10 atom%	p	—	6–8	—	10^3

Pine RDE 3 potentiostat enabling us to study the sample either under potentiostatic or potentiodynamic conditions. All results on dark and photocurrents presented in this work have been obtained under potentiostatic steady state conditions.

Illumination of the sample was provided by a 500 W Tungsten halogen lamp focused with quartz optics and with most of the infrared radiation absorbed by a 5-cm water cell. A visible pass filter (Corning 3-72) allowed photons with $h\nu \leq 2.7$ eV to illuminate the sample. The irradiance was measured with a thermopile detector. When we take into account the slight absorption of light by the pass filter and by the electrolyte the incoming power was 35 mW on a 1 cm^2 surface area.

A gas chromatograph (Hewlett-Packard 5720 A) fitted with a thermal conductivity detector and a molecular sieve 5A column was used to detect H_2 produced in the cell. Calibration of the gas chromatograph was carried out by injecting small but well-defined doses of H_2 and O_2 directly into the cell. The detection limit corresponds to a production rate in the cell of 10^{16} H_2 molecules/hr. The detection limit for O_2 is 15

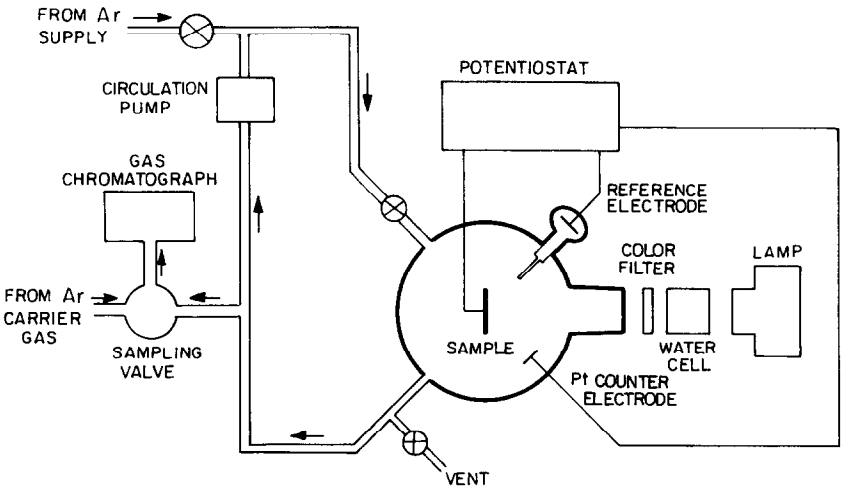

FIG. 2. Apparatus for simultaneous photocurrent and gas evolution studies. The electrochemical cell is viewed from above.

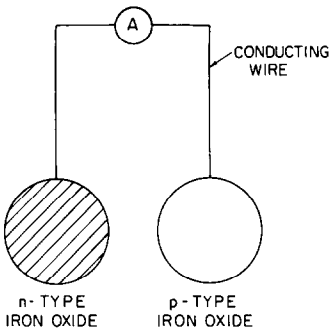

FIG. 3. p/n-type iron oxide assembly.

times higher. Direct measurements of photoinduced O_2 production were difficult, however, because of high leak rates (of the order of 10^{17} O_2 molecules/min) into the cell and loop system. The closed loop contains Ar to carry H_2 from the cell through a sampling valve to the gas chromatograph. The gas is circulated by means of a mechanical pump fitted with Teflon gears. Blank experiments involving only the electrolyte and a sample holder in the cell gave no indication of H_2 produced, either in the dark or under illumination.

To connect the sample to the potentiostat a Ni wire was attached to one side of each sample with Ag epoxy. Silicon rubber sealant was used to insulate the wire and the epoxy from the electrolyte solution. In later experiments p- and n-type iron oxide samples were connected by means of a Ni wire and a microammeter (Fig. 3) which enabled us to measure the photoinduced current between the samples in addition to measuring the amount of hydrogen evolved from the p-type iron oxide. These experiments were carried out in the same cell as before but without using the potentiostat.

The consistency of the H_2 calibration was checked by comparing the number of H_2 molecules detected with the gas chromatograph with the integrated photocurrent through the sample after various times. This was done on $SrTiO_3$ and TiO_2 single crystals. The results shown in Fig. 4 are from $SrTiO_3$ polarized at 100 mV (RHE). The dashed line corresponds to the expected number of H_2 molecules according to Faraday's Law and assuming that the formation of H_2 is the only cathodic reac-

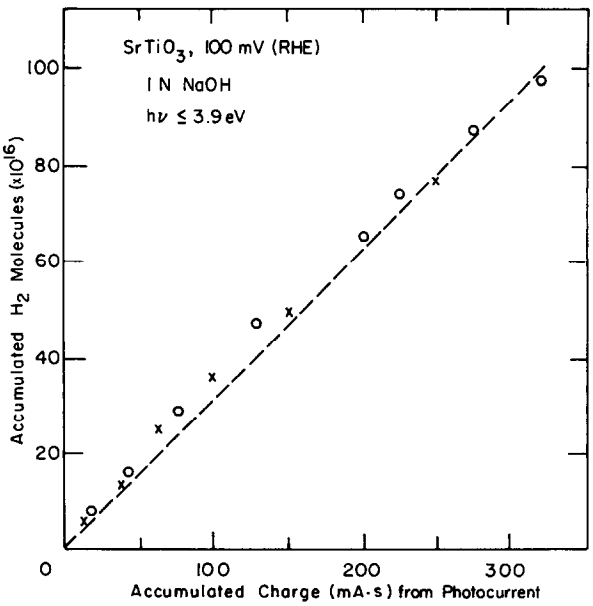

FIG. 4. Accumulated number of H_2 molecules as measured with gas chromatography vs photoinduced charge across a $SrTiO_3$ single crystal at 100 mV (RHE) in 1 *N* NaOH. Crosses and circles are data points from two different runs. Dashed line is the expected result according to Faraday's Law.

tion. The agreement between the calibrated experimental data and expected values is very good, generally within ±5%.

3. RESULTS

We first present results of the photoelectrochemical measurements using n-type and p-type iron oxide samples separately and then the photochemical studies using the p/n diode assembly. An important parameter to consider is the onset potential for the production of photocurrent. If a photoinduced current is to occur between an n-type and a p-type sample without any applied potential, a necessary condition is that the onset potential of the n-type sample is less (more cathodic) than that of the p-type sample. Consequently, in what follows, emphasis is put on presenting the onset potential for photocurrent production in addition to values of photocurrents in various solutions and for differently doped iron oxides.

3.1. Photoelectrochemical Properties of n-Type Si-Doped Iron Oxides

In Fig. 5 the photocurrent of an Si-doped iron oxide (Si/(Si + Fe) = 2 atom%) is shown in both 0.1 *M* Na_2SO_4 (pH 6) and 0.01 *N* NaOH (pH 12). Similar measurements were also performed in distilled water (pH 8) and in 1 *N* NaOH (pH 14). A comparison between photocurrents obtained in different NaOH solution supports earlier observations on n-type $SrTiO_3$ in which the photoactivity increases with the pH of the solution (*7*). Dark currents were low and never exceeded 10 μA/cm² in the potential region shown here.

From Fig. 5 an onset potential for photocurrent production can be extracted. This has been defined as the lowest potential where a photocurrent of 0.5 μA/cm² is observed. Table 2 (middle column) displays the onset potential of Si-doped iron oxides in 0.01 *N* or 1 *N* NaOH as a function of the atom fraction of Si. The onset potential drops from 0.725 ± 0.025 to 0.600 ± 0.025 V (RHE) upon introduction of 1 atom% Si and stays at this value with increasing Si concentration. Above 20 atom% Si the onset potential rises again. Within the error bars these results hold true in both 0.01 *N* NaOH and 1 *N* NaOH with a tendency for the onset potential to be slightly less in the 1 *N* NaOH solution.

The onset potential for photocurrent production can be further lowered by preoxidizing the n-type iron oxide surface. This has been accomplished either by anodic po-

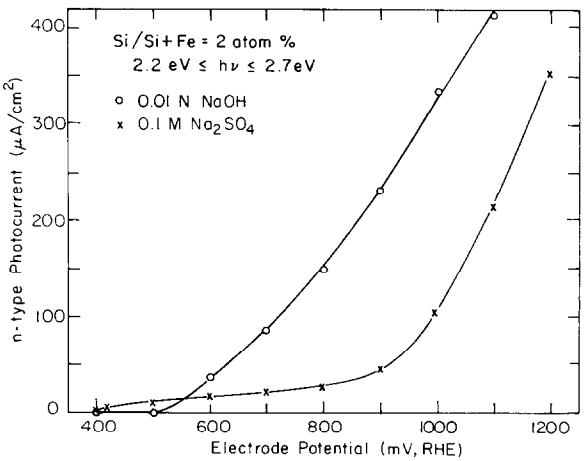

FIG. 5. Photocurrent density as a function of electrode potential for Si-doped iron oxide in 0.01 *N* NaOH and in 0.1 *M* Na_2SO_4. Si/Si + Fe = 2 atom%. Dark currents never exceeded 10 μA/cm² in the potential region shown here.

TABLE 2

Onset Potential (mV, RHE) for Photocurrent Production of Iron Oxide with Different Atomic Fractions of Si

Si/(Si + Fe) (atom%)	Onset potential in 1 *N* NaOH and 0.01 *N* NaOH (mV, RHE)	Onset potential after preoxidation treatment (O_2 purging at 60–80°C) in 1 *N* NaOH (mV, RHE)
0	725 ± 25	650 ± 50
1	600 ± 25	500 ± 50
2	600 ± 25	450 ± 50
3	625 ± 25	475 ± 50
5	600 ± 25	450 ± 50
10	650 ± 25	575 ± 50
20	650 ± 25	600 ± 50
50	700 ± 25	

larization of the sample at potentials above 900 mV (RHE) or by purging the solution with oxygen at temperatures in the range of 60 to 80°C. With both oxidizing pretreatments a decline in onset potential is observed in the range of 100–200 mV for most Si-doped iron oxides studied. Thus, the combination of Si doping and preoxidation of the iron oxide samples decreases the onset potential by 100 to 300 mV as compared to undoped n-type iron oxide (see Table 2, right column). ESCA studies show an increase in oxidation state of Fe after the preoxidation treatment, which could be correlated with the observed shift in onset potential for photoproduction (*8*).

3.2. Photoelectrochemical Properties of p-Type Mg-Doped Iron Oxides

The solutions in which the Mg-doped iron oxides were tested include 0.1 *M* Na_2SO_4, 0.01, 1, and 3 *N* NaOH, 0.5 *M* NaCl, and distilled water. The photocurrents in the NaOH solutions increased with decreasing pH (as opposed to the behavior of n-type samples which exhibit decreased photocurrent with dilution, see previous section) but were poor in distilled water. In Fig. 6 the photocurrents are given for four Mg-doped iron oxides in the 0.01 *N* NaOH solution. The 10% doping appears to give the best results although the 5, 10, and 20% samples essentially produce equivalent photocurrents. As seen in Fig. 7 the photocurrents in 0.1 *M* Na_2SO_4 are of the same magnitude as in 0.01 *N* NaOH. Again, the three higher doping levels appear to give similar results whereas 1% Mg doping produces lower photocurrents. During prolonged polarization no poisoning of the photoactivity was observed. While polarizing an Mg-doped sample (Mg/(Mg + Fe) = 5 atom%) at 600 mV (RHE) the photocurrent in the 0.01 *M* NaOH solution increased over an 8-hr period by 50% and in the 0.1 *M* Na_2SO_4 solution by 30% in the same time span. Dark currents are not shown in Figs. 5 and 6 but were relatively high, almost of the same order of magnitude as the photocurrents shown. In the NaCl solution both

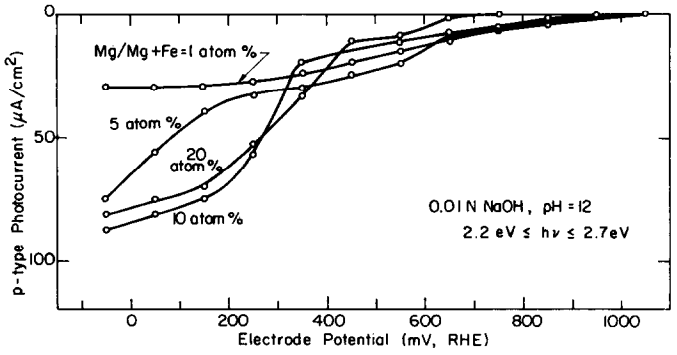

FIG. 6. Photocurrent density as a function of electrode potential for various Mg-doped iron oxides in 0.01 *N* NaOH. At each potential the magnitude of the dark current was within 25% of the photocurrent.

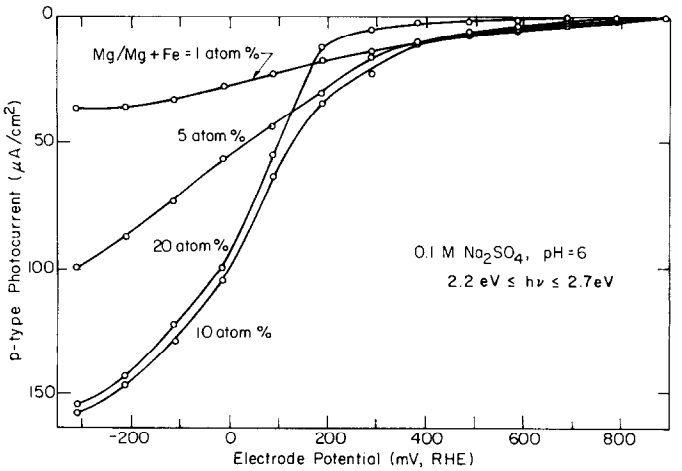

FIG. 7. Photocurrent density as a function of electrode potential for various Mg-doped iron oxides in 0.1 *M* Na_2SO_4. At each potential the magnitude of the dark current was within 25% of the photocurrent.

the dark and light currents for all samples were unstable and visible poisoning of the samples occurred almost instantaneously.

Table 3 shows the measured onset potentials for photocurrent production in 0.01 *N* NaOH and in 0.1 *M* Na_2SO_4. In both solutions the three lower Mg dopant levels give similar onset potentials, while the 20% Mg-doped sample exhibits 200–300 mV lower onset potentials.

The effect of the gases N_2, CO_2, and O_2 passed through the solution was relatively independent of the electrolyte used or the doping level of Mg. Purging the electrolyte solution with CO_2 caused a rapid decay in the photocurrent which led to the poisoning of the photodissociation of water. N_2 produced no measurable effect, while the presence of oxygen greatly improved, more than doubled, the photocurrent. In the NaOH or in the Na_2SO_4 solutions poisoning of the p-type iron oxides occurs after 6–8 hr of exposure when connected with an n-type iron oxide (see the next section). Oxygen introduced after a sample had been poisoned aided in reoxidizing the cathode and regenerating a photocurrent comparable to the original photocurrent before poisoning.

TABLE 3

Onset Potential (mV, RHE) for Photocurrent Production of Iron Oxide with Different Atomic Fractions of Mg

Mg/(Mg + Fe) (atom%)	Onset potential in 0.01 *N* NaOH (mV, RHE)	Onset potential in 0.1 *M* Na_2SO_4 (mV, RHE)
1	1000 ± 50	850 ± 50
5	950 ± 50	825 ± 50
10	950 ± 50	850 ± 50
20	725 ± 50	650 ± 50

3.3. p- and n-Type Iron Oxide Assemblies

As shown in previous sections the onset potential for photocurrent production of n-type Si-doped iron oxides was less (more cathodic) than that of the best p-type Mg-doped iron oxides. When connecting n-type and p-type iron oxides by a conducting wire over a microammeter one could then expect a certain photocurrent to flow between the n-type and p-type iron oxides. We have prepared p/n iron oxide diode assemblies with an n-type iron oxide that contains Si/(Si + Fe) = 2 atom%, whereas the Mg dopant level in the p-type iron oxide is varied between 1 and 20 atom%. The photoactivity of the p/n assembly in different aqueous so-

lutions can be measured either by monitoring the photocurrent or the hydrogen evolution from the p-type sample. Table 4 gives measured photocurrents of p/n iron oxide assemblies with different Mg contents. The results are based on 1 hr of exposure in 0.01 *N* NaOH and in the absence of an external potential. Values of photocurrents are shown when both samples are illuminated and when either the n-type or the p-type iron oxide is illuminated alone. Illuminating both samples gives photocurrents which in general are higher than the sum of the photocurrents produced when only illuminating either the n-type or the p-type sample. A similar cooperative effect has been observed and discussed elsewhere (*5*). Variation in photocurrents during 1 hr were typically within ±5%. As seen in Table 4 a dark current was observed which was below 0.5 μA and which decreased with time to less than 0.1 μA after 10–20 hr of exposure. When photoinduced H_2 production rates were measured in addition to photocurrents an agreement within ±25% was found as seen in Table 5 with a slight tendency for the H_2 production rates to be less than expected from photocurrent measurements. (Following Faraday's Law and assuming no reactions other than the production of H_2 on the p-type sample, a photocurrent of 1 μA would correspond to a H_2 production rate of about 1.1×10^{16} H_2 molecules/hr.) Hence steady-state rates of H_2 in the range of one monolayer (≃10^{15} H_2 molecules) per minute could be sustained for hours in both 0.01 *N* NaOH and 0.1 *M* Na_2SO_4 in the absence of any external potential.

TABLE 4

Measured Photocurrents in p/n Iron Oxide Assemblies after 1 hr of Exposure in 0.01 *N* NaOH[a]

Photocurrent (μA)	Mg/(Mg + Fe) (atom%)			
	1	5	10	20
Both n- and p-type illuminated	5	8	13	3
Only n-type illuminated	2.5	2.5	3.5	2.5
Only p-type illuminated	1.5	1.5	4	0.5
No illumination	<0.5	<0.5	<0.5	<0.5

[a] n-type, Si/(Si + Fe) = 2 atom%; p-type; Mg/(Mg + Fe) = 1, 5, 10, and 20 atom%.

TABLE 5

Measured Photocurrents and H_2 Production Rates in p/n Iron Oxide Assembly after 1 hr of Exposure in 0.01 *N* NaOH and 0.1 *M* Na_2SO_4[a]

	0.01 *N* NaOH	0.1 *M* Na_2SO_4
Both samples illuminated		
Photocurrent (μA)	8 ± 1	6 ± 1
H_2 production rate (10^{16} molecules/hr)	6 ± 0.5	5 ± 0.5
H_2 production rate (10^{16} molecules/hr) equivalent to measured photocurrent	8.8 ± 1	6.6 ± 1

[a] n-type, Si/(Si + Fe) = 2 atom%; p-type, Mg/(Mg + Fe) = 5 atom%.

After about 6–8 hr of exposure in both NaOH and Na_2SO_4 the H_2 production rate and the photocurrent in the p/n iron oxide assembly declined. Subsequent separate photoelectrochemical measurements showed that the photoactivity of the p-type iron oxide had declined in proportion, while the photoactivity of the n-type sample remained unchanged. The partly deactivated assembly could be readily regenerated by flowing oxygen through the solution at room temperature for 1–20 min. Using this treatment both the H_2 production and the photocurrent returned to their original higher values.

4. DISCUSSION

We have clear evidence that hydrogen can be produced from water by connecting p- and n-type iron oxides. This was accomplished by using visible light (2.2 eV ≤ $h\nu$ ≤ 2.7 eV) and in the absence of an applied potential. When allowing the p-type sample to be regenerated by O_2 purging every 4–6 hr, a steady-state rate of 1–2 monolayers of H_2/min was obtained at 300 K yielding

about 3000 monolayers ($\approx 10^{-5}$ mole) per 24 hr. Thus the process is catalytic.

It is important to note that the onset potential for detecting photocurrents for the best p-type Mg-doped iron oxides using a potentiostat and a Pt counter electrode is around 300–400 mV higher (more anodic) than for the best n-type Si-doped iron oxides. From the electronegativities of Mg (1.2), Si (1.8), and Fe (1.7) and following the scheme outlined by Butler and Ginley (*9*), one would expect a flatband potential for the Mg-doped iron oxides to be less (more cathodic) than that of Si-doped iron oxides—in contrast to our result. However, other factors such as the presence of surface recombination centers (*10*), chemisorption of ions causing changes in the Helmholtz layer (*11*), or the oxidation state of the cation in the semiconductor (*8, 12*) may all cause deviations of onset potentials from predicted values when using strictly electronegativity arguments.

After 6–8 hr the rate of hydrogen evolution diminished along with the photocurrent from the p-type Mg-doped iron oxide. Regeneration of the partially deactivated sample could be carried out by the introduction of a slow stream of oxygen into the reaction chamber. Upon this oxygen exposure that lasts for minutes at 300 K, both H_2 production and the photocurrent of the p-type iron oxide cathode returned to their original higher value. Thus, it appears that the slow deactivation is due to the reduction of the p-type iron oxide as a fraction of the hydrogen that is produced remains on its surface to participate in surface reactions.

The beneficial effect of Si doping on the photoelectrochemical behavior of iron oxide is in agreement with previously reported work on sintered iron oxides prepared in a similar way (*13*). Introduction of 1 atom% of Si increases the conductivity of the iron oxide by at least three orders of magnitude and also reduces the onset potential for photocurrent production by more than 100 mV (Table 2). Higher Si dopings than 5 atom% seem to have no significant beneficial effect, which at least partly can be explained by smaller widths of the depletion layer in heavily doped semiconductors. A similar explanation can be given for the dependence of onset potential on Mg doping, which is less favorable for the highest Mg-doping level (Table 3). The need for high quantum efficiencies and, hence, larger widths of the depletion layer would suggest the use of iron oxides with the lowest possible dopant levels. The need for a low p/n cell resistivity is satisfied with higher Mg dopant levels (Table 1). Taking into account the onset potentials of Mg- and Si-doped electrodes as well as their resistivities, one would expect an optimum p/n cell performance at Mg-doping levels somewhere between 1 and 20 atom% Mg. In agreement with these arguments we find higher photocurrents for 5 and 10 atom% Mg than for 1 and 20 atom% Mg (see Table 4).

Whereas photoelectrochemical measurements gave very low dark currents (below 10 $\mu A/cm^2$ at the highest potentials investigated) for Si-doped iron oxides, corresponding measurements on Mg-doped iron oxides showed much higher dark currents, around 100 $\mu A/cm^2$ at the lowest potentials investigated. However, when connecting Mg- and Si-type iron oxides to form p/n assemblies the dark current between the pair of samples was in general below 0.5 μA during the first hour and one order of magnitude lower after several days of exposure. In accordance with this, AES measurements did not reveal any significant changes in surface composition after long exposures (>1 hr) of the samples to NaOH solutions.

The chemical output power of the polycrystalline p/n iron oxide assembly can be calculated either from the photoinduced hydrogen production rate or from the measured photocurrents across each p/n assembly using photon energies in the solar range. Based on the free energy change when H_2 is produced from H_2O the output power is equal to $1.23 \times i$ μW where i is the

measured photocurrent in μA. Using 13 μA as the photocurrent obtained for the best p/n assembly listed in Table 3 and an input power of 35 mW, a power conversion efficiency of around 0.05% is obtained. This can be compared with other p/n photoelectrolytic cells in which efficiencies were reported which were one order of magnitude higher (*3, 4*). It should be noted, however, that these cells contained single crystal TiO_2 (Eg = 3.0 eV) or $SrTiO_3$ (Eg = 3.2 eV) as n-type electrodes and required considerably higher photon energies than the present cell that make them unlikely candidates for photochemical solar energy conversion.

A photocatalytic device as outlined here is capable of generating H_2 and O_2 in two separate compartments. Solar power can be transformed into either chemical energy (by collecting H_2) or into electrical energy by utilizing the photocurrent between the p- and n-type iron oxide electrodes.

The photoactivity of the p/n iron oxide assembly used at present can be improved in several ways. Photoelectrochemical measurements of these sintered Mg- and Si-doped iron oxide pellets so far reveal relatively low photocurrents. An important factor to consider here is the presence of grain boundaries which are known as efficient electron-hole recombination sites. Preliminary measurements have shown that increasing the sintering temperature by 50°C during the preparation of the doped iron oxide discs increased the grain size of the Si-doped iron oxide samples from about 10–20 to about 50–100 μm, which resulted in significantly higher photocurrents. Deposition of Pt with thickness >20 nm has been attempted to aid the hydrogen atom recombination at the p-type iron oxide but has so far shown no beneficial affect on the hydrogen production rate. In fact, when Pt was deposited in the form of a grid over the p-type iron oxide surface the photocurrent deteriorated and the hydrogen production rate also declined in proportion. Improvement in the rate of H_2 evolution may, however, be found when depositing considerably thinner Pt layers. Modifications in the architecture of the cell or of the p/n assembly as well as changes in dopants or dopant levels of primarily the p-type iron oxide could further increase the photocurrents and thus the power conversion efficiency. Construction of a leak tight cell will permit O_2 detection as well as H_2 detection in order to establish stoichiometry.

A turnover rate of 10^{-2} molecules per site per second at 300 K to produce H_2 is of the same order of magnitude as the rates for many hydrocarbon reactions over metal catalyst surfaces in the range of 500 to 700 K. Thus, even under present conditions the hydrogen production by the photocatalyzed dissociation of water could have been the precursor of surface reactions with CO_2 or CO to produce hydrocarbons. In addition, iron and its compounds are excellent catalysts for the hydrogenation of CO and CO_2 to produce hydrocarbons and for the water gas shift reaction ($CO + H_2O \rightarrow CO_2 + H_2$) (*14*). Iron readily dissociates N_2 by a structure sensitive reaction (*15*), providing means for the incorporation of nitrogen into organic molecules.

ACKNOWLEDGMENTS

This work was supported by the Director, Office of Energy Research, Office of Basic Energy Sciences, Chemical Sciences Division of the U.S. Department of Energy under Contract DE-AC03-76SF00098. We are indebted to G. Lewis and D. Neiman for assisting in sample preparation.

REFERENCES

1. Hardee, K. L., and Bard, A. J., *J. Electrochem. Soc.* **124,** 215 (1977).
2. Yoneyama, H., Sakamoto, H., and Tamura, H., *Electrochim. Acta* **20,** 341 (1975).
3. Nozik, A. J., *Appl. Phys. Lett.* **30,** 567 (1977).
4. Okashi, K., McCann, J., and Bockris, J. O'M., *Nature (London)* **266,** 610 (1977).
5. Mettee, H., Otvos, J. W., and Calvin, M., *Solar Energy Mater.* **4,** 443 (1981).
6. Shinar, R., and Kennedy, J. H., *Solar Energy Mater.* **6,** 323 (1982).
7. Wagner, F. T., and Somorjai, G. A., *J. Amer. Chem. Soc.* **102,** 5474 (1980).

8. Leygraf, C., and Somorjai, G. A., to be published.
9. Butler, M. A., and Ginley, D. S., *Chem. Phys. Lett.* **47,** 319 (1977).
10. Wilson, R. H., *J. Appl. Phys.* **48,** 4292 (1977).
11. Wilson, J. R., and Park, S.-M., *J. Electrochem. Soc.* **128,** 2369 (1981).
12. Sayers, C. N., and Armstrong, N. R., *Surface Sci.* **77,** 301 (1978).
13. Kennedy, J. H., Shinar, R., and Ziegler, J. P., *J. Electrochem. Soc.* **127,** 2307 (1980).
14. Newsome, D. S., *Catal. Rev.-Sci. Eng.* **21,** 275 (1980).
15. Spencer, N. D., Schoonmaker, R. C., and Somorjai, G. A., *J. Catal.* **74,** 129 (1982).